

Southern Ocean seabird population shifts over the Holocene revealed by peat sequestration of mercury from guano

Chuxian Li

`chuxian.li@slu.se`

Swedish University of Agricultural Sciences <https://orcid.org/0000-0002-5458-3171>

Stephen Roberts

British Antarctic Survey <https://orcid.org/0000-0003-3407-9127>

Martin Grosjean

University of Bern <https://orcid.org/0000-0002-3553-8842>

Adrien Mestrot

University of Bern <https://orcid.org/0000-0002-4387-3886>

Martin Wille

Institut für Geologie, Universität Bern

Richard Phillips

British Antarctic Survey, Natural Environment Research Council

Maxime Enrico

<https://orcid.org/0000-0002-9322-7057>

Kevin Bishop

Swedish University of Agricultural Sciences <https://orcid.org/0000-0002-8057-1051>

Ulf Skjellberg

Swedish University of Agricultural Sciences <https://orcid.org/0000-0001-6939-8799>

Dmitri Mauquoy

University of Aberdeen <https://orcid.org/0000-0002-8056-8258>

Clemens von Scheffer

University of Aberdeen

Thomas Theurer

University of Aberdeen

David Muirhead

University of Aberdeen

Alex Whittle

British Antarctic Survey

Angela Gallego-Sala

University of Exeter <https://orcid.org/0000-0002-7483-7773>

Jeroen Sonke

CNRS & University of Toulouse <https://orcid.org/0000-0001-7146-3035>

François de Vleeschouwer

Universidad de Buenos Aires

Nathalie Putten

Earth and Climate Cluster, Faculty of Science, Vrije Universiteit, Amsterdam

Pascale Braconnot

LSCE-IPSL <https://orcid.org/0000-0002-1852-9178>

Olivier Marti

CEA <https://orcid.org/0000-0002-8246-5578>

Stefan Osterwalder

University of Zurich

Nina Buchmann

ETH Zurich <https://orcid.org/0000-0003-0826-2980>

Thomas Frölicher

University of Bern <https://orcid.org/0000-0003-2348-7854>

Eva Anthamatten

University of Bern

Aurea Chiaia-Hernández

University of Bern

Petra Zahajská

University of Bern

Catherine Jeandel

CNRS <https://orcid.org/0000-0002-4915-4719>

Krystyna Saunders

ANSTO <https://orcid.org/0000-0002-6800-2630>

Sae Yun Kwon

Pohang University of Science and Technology <https://orcid.org/0000-0001-8665-0327>

Dingyong Wang

Southwest University <https://orcid.org/0000-0003-1157-7617>

Richard Bindler

Umeå University <https://orcid.org/0000-0002-7900-309X>

Louise Sime

British Antarctic Survey <https://orcid.org/0000-0002-9093-7926>

Dominic Hodgson

British Antarctic Survey

Keywords:

Posted Date: October 1st, 2025

DOI: <https://doi.org/10.21203/rs.3.rs-7749632/v1>

License:   This work is licensed under a Creative Commons Attribution 4.0 International License.

[Read Full License](#)

Additional Declarations: There is **NO** Competing Interest.

Southern Ocean seabird population shifts over the Holocene revealed by peat sequestration of mercury from guano

Chuxian Li ^{1,2*}, Stephen J. Roberts ³, Martin Grosjean ¹, Adrien Mestrot ¹, Martin Wille ⁴, Richard A. Phillips ³, Maxime Enrico ⁵, Kevin Bishop ², Ulf Skyllberg ⁶, Dmitri Mauquoy ⁷, Clemens von Scheffer ⁷, Thomas Theurer ⁷, David Muirhead ⁷, Alex Whittle ^{3,8}, Angela Gallego-Sala ⁸, Jeroen E. Sonke ⁹, François de Vleeschouwer ¹⁰, Nathalie Van der Putten ¹¹, Pascale Braconnot ¹², Olivier Marti ¹², Stefan Osterwalder ¹³, Nina Buchmann ¹⁴, Thomas Frölicher ¹⁵, Eva Anthamatten ¹, Aurea C. Chiaia-Hernández ¹, Petra Zahajská ¹, Catherine Jeandel ¹⁶, Krystyna M. Saunders ¹⁷, Sae Yun Kwon ¹⁸, Dingyong Wang ¹⁹, Richard Bindler ²⁰, Louise Sime ³, Dominic A. Hodgson ³

*Corresponding author: chuxian.li@slu.se

Affiliations

1. Institute of Geography and Oeschger Center for Climate Change Research, University of Bern, Bern 3012, Switzerland
2. Department of Aquatic Sciences and Assessment, Swedish University of Agricultural Sciences, Uppsala 75007, Sweden
3. British Antarctic Survey, Natural Environment Research Council, High Cross, Madingley Road, Cambridge, UK
4. Institute of Geological Sciences, University of Bern, Bern, Switzerland
5. Université de Pau et des Pays de l'Adour, E2S UPPA, CNRS, IPREM, Pau 64000, France
6. Department of Forest Ecology and Management, Swedish University of Agricultural Sciences, Umeå, Sweden
7. School of Geosciences, University of Aberdeen, Scotland, UK
8. Geography Department, University of Exeter, Exeter, UK
9. Laboratoire Géosciences Environnement Toulouse, Université de Toulouse, CNRS, INPT, UPS, Castanet Tolosan, France
10. Instituto Franco-Argentino para el Estudio del Clima y sus Impactos (UMI 3351 IFAECI/CNRS-CONICET-IRD-UBA), Universidad de Buenos Aires, Argentina
11. Department of Earth Sciences, Vrije Universiteit Amsterdam, Amsterdam, The Netherlands
12. Laboratoire des Sciences du Climat et de l'Environnement, LSCE/IPSL, CEA-CNRS-UVSQ, Université Paris-Saclay, Gif-sur-Yvette, France
13. Department of Geography, Hydrology and Climate, University of Zurich, Zurich, Switzerland
14. Grassland Sciences, Institute of Agricultural Sciences, ETH Zürich, Zürich, Switzerland
15. Climate and Environmental Physics, Physics Institute, University of Bern, Bern, Switzerland
16. LEGOS, Université de Toulouse, CNES, CNRS, IRD, Toulouse, France
17. Australian Nuclear Science and Technology Organisation, Lucas Heights, New South Wales, Australia
18. Division of Environmental Science and Engineering, Pohang University of Science and Technology, Pohang, Republic of Korea
19. College of Resources and Environment, Southwest University, Chongqing 400715, China
20. Department of Ecology and Environmental Science, Umeå University, Umeå, Sweden

Abstract

Monitored seabird populations have declined by up to 70% worldwide since the 1950s, yet little is known about population sizes or long-term trends prior to anthropogenic impacts. This is particularly true for the Southern Ocean, where seabirds and many other species are currently facing multiple environmental threats. Here, we identify shifts in seabird populations over the last 8100 years by applying a mercury (Hg) flux and isotope signature technique as a novel tracer of population size via guano input into peatlands on sub-Antarctic Bird Island (South Georgia). Our results show that seabirds have colonized Bird Island between 6800 and 6100 years ago, which pre-dates evidence for colonization of other sub-Antarctic islands by more than 1000 years. There are five periods when seabird populations were at maxima during the mid- to late-Holocene, coeval with periods of lower Southern Hemisphere westerly wind intensity. Our study provides unprecedented insights into cyclicity in seabird population sizes as a consequence of regional to large-scale environmental change.

52 **Keywords:** seabird populations, climate change, Holocene, peat, mercury

53

54 **Introduction**

55

56 Monitored seabird populations have declined globally by ~70% between 1950 and 2010¹ due to a
57 range of human activities, such as overfishing of food sources, pollution, climate change, and
58 incidental mortality (bycatch) in fishing gear, particularly in the Southern Hemisphere². These rapid
59 declines threaten wider ecosystem structure and function, because seabirds provide ecological
60 services, including energy and nutrient transport and cycling³. Seabirds are also excellent indicators
61 of spatiotemporal changes in marine ecosystem health since they are long-lived, wide-ranging, and
62 forage at high trophic levels⁴.

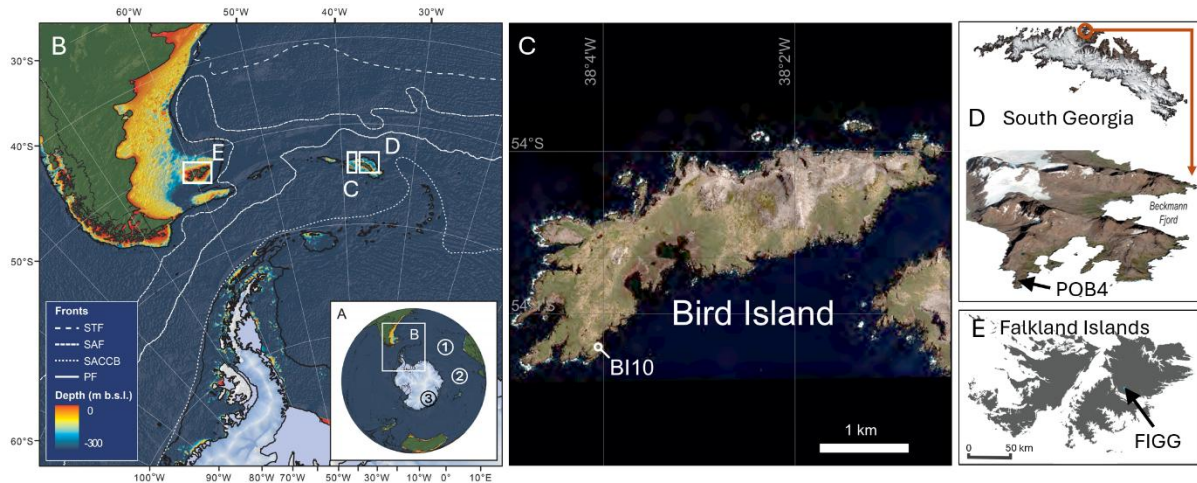
63 The Southern Ocean is an area of high conservation priority because it is the foraging area for very
64 large seabird populations⁵, including many threatened species². Numerous Southern Ocean seabird
65 species are projected to decline further in response to future climate change, such as increased sea
66 surface temperature and decreased sea-ice extent⁶ that reduce survival rates and breeding
67 performance⁶⁻⁹. Current monitoring of seabird population sizes and trends largely relies on counts in
68 the field, digital image analysis (from satellites, aircraft or drones)¹⁰, or acoustic loggers for some
69 burrowing species^{11,12}. However, almost all monitoring programs started in the last few decades, and
70 are therefore not able to determine longer-term impacts of natural and anthropogenic drivers. This
71 limits our understanding of pre-industrial baselines and ability to develop longer-term (decadal scale)
72 mitigation plans or assess the range of natural pressures on seabird populations.

73 Biogeochemical analysis of natural archives, such as lake sediments and peat cores, offers
74 opportunities to fill this knowledge gap by providing long-term reconstructions of changing seabird
75 populations¹³. Many Southern Ocean seabirds breed on islands where there are lakes, ponds, and
76 peatlands. Seabirds feed on crustaceans (e.g., Antarctic krill, *Euphausia superba*), cephalopods, and
77 fish¹⁴⁻¹⁶, and when back at their breeding and roosting sites excrete guano that is enriched in nutrients
78 and bio-elements (e.g., N, C, P, Fe, Cu, Se, Co, Ni, Zn, Mn); these can facilitate plant growth and peat
79 formation¹⁷. Guano can also be transported through runoff and seepage into coastal waters, and
80 lakes, where elements are preserved in sediments^{18,19}.

81 Several studies of lake sediment records from the Northern Hemisphere^{13,20-25} and Antarctica^{19,26,27}
82 have shown seabird population changes in response to climate, ecosystem shifts, explosive volcanism,
83 or anthropogenic influences. For example, geochemical and biomarker methods applied to an 8.5-ka
84 lake sediment profile from Ardley Island revealed that a penguin colony was established following
85 warm conditions on the northern Antarctic Peninsula c. 6.7 ka BP, which is the earliest known for the
86 region¹⁹. Data on seabird population trends prior to the 1950s are limited, and information derived
87 from peat deposits is even rarer, with only three relevant studies available to date^{17,25,28}. Two studies
88 that are largely based on permafrost cores show different timing of seabird presence at different
89 coastal areas in northwest Greenland^{25,28}, including the first recorded arrival of the little auk (*Alle alle*)
90 at c. 4.4 ka BP in the Annikitsoq area²⁵. In the Southern Ocean, a peat core from the east coast of the
91 Falkland Islands indicates colonization by seabirds c. 5 ka BP during a period of regional cooling¹⁷. The
92 past seabird information from all three peat studies largely relies on bio-elements^{17,25} and stable
93 isotopes (C, N)²⁸, in addition to grass pollen and charcoal proxies¹⁷. However, some bio-elements
94 might not be widely applicable as tracers for seabird presence in peatland deposits because of their
95 role in metabolism. These bio-elements can be recycled by vegetation during peat decomposition,
96 possibly obscuring the signals of guano deposition at the time of peat formation.

97 Mercury (Hg) is a non-essential trace element that can be a suitable tracer for the incorporation of
98 guano into peat deposits. This element bioaccumulates in marine organisms, and biomagnifies
99 through trophic levels, ultimately reaching high concentrations in top predators such as seabirds^{29,30}.
100 Seabird guano input enhances Hg concentrations in peatlands compared to unoccupied sites, leading
101 to high Hg loads at breeding colonies³¹⁻³³. For example, a mean total Hg (THg) concentration of
102 $114 \pm 50 \text{ ng g}^{-1}$ ($n = 43$) was recorded in deposited guano from a colony of herring gulls *Larus*
103 *argentatus* on a peatland surface in North America³³. This is three times higher than the mean THg
104 concentration in a remote, uncolonised peatland ($37 \pm 34 \text{ ng g}^{-1}$, $n = 101$)³⁴, which mainly receives Hg
105 from atmospheric deposition. Vegetational sequestration of gaseous element Hg^0 , the dominant form
106 of Hg in the atmosphere, is the main deposition pathway of Hg to peatlands in the absence of avian
107 influence³⁵. Once taken up by vegetation, Hg^0 is oxidized to Hg^{II} via intra-cellular enzymatic reactions
108 or by reactive oxygen species³⁶. Rainfall also contributes Hg^{II} to peatlands, but at lower rates (e.g.,
109 20 – 30% of total atmospheric Hg^{34,35,37}). Deposited Hg^{II} from rainfall, or produced by oxidation of
110 Hg^0 associated with plant uptake, forms thermodynamically stable complexes with thiol groups of
111 decomposing organic matter in peat, potentially forming immobile nanoparticulate $\beta\text{-HgS}$ ³⁸. The
112 strong affinity of Hg^{II} to organic matter thiols makes it less susceptible to reduction back to Hg^0 ³⁹, thus
113 Hg in peatlands has the potential to reflect input from both the atmosphere and guano⁴⁰. Additionally,
114 the Hg stable isotope signatures of atmospheric Hg^0 , rainfall Hg^{II} , and guano Hg are distinct^{27,34},
115 enabling quantification of these input sources to peat.

116 In this study, we apply Hg flux and stable isotope analysis to peatland deposits found on sub-Antarctic
117 Bird Island, a small island at the western end of the South Georgia island group (Fig. 1). South Georgia
118 holds globally important breeding populations of seabirds, including several small but highly abundant
119 burrowing petrel species, as well as threatened albatross, petrel and penguin species listed by the
120 *International Union for the Conservation of Nature* because of steep population declines^{2,41}. Our main
121 study site at Bird Island, BI10, is a valley peatland that dates back c. 8.1 ka ago. The BI10 site receives
122 water largely from surface drainage, with a high water table sustained through gravitational lateral
123 seepage from adjacent slopes^{42,43}. Guano from seabirds breeding on these slopes is transported from
124 the catchment to the BI10 peatland site. For reference, we investigated changes in Hg at two control
125 sites in the absence of large resident bird colonies: 1) POB4, a highly minerotrophic peatland profile
126 was taken from the Prince Olav Harbour Bog on nearby mainland South Georgia, and 2) FIGG, a peat
127 profile was taken 12 km east of Goose Green on the Falkland Islands. The POB4 profile includes a
128 (lacustrine) sediment sequence at its base and is dated between c. 4.5 – 8.5 ka BP (Supplementary
129 note 1; Supplementary Figs. S1, S2). All the peat profiles examined in this study were undisturbed and
130 increased in thickness over time, providing a continuous record of the environmental conditions
131 prevailing at the time of peat formation⁴⁴.



132

133 **Fig. 1:** (A) Map of the Southern Hemisphere, highlighting sub-Antarctic regions where peatlands were
 134 sampled for this study. ①, ②, ③ show sea-ice records from Nielsen et al., (2004)⁴⁵, Orme et al.,
 135 (2020)⁴⁶, and Röthlisberger et al., (2002)⁴⁷, respectively. (B) Map of the southwest Atlantic sector of
 136 the Southern Ocean, showing the locations of our three peatland study sites: Bird Island, South
 137 Georgia (C, BI10 site), mainland South Georgia (D, POB4 site), and the Falkland Islands (E, FIGG site).
 138 Major oceanic fronts where seabirds can forage are shown in (B), including the Subtropical Front (STF),
 139 Subantarctic Front (SAF), Southern Antarctic Circumpolar Current Boundary (SACCB), and the Antarctic
 140 Polar Front (PF).

141 **Results and Discussion**

142 **Holocene Hg accumulation rates at sub-Antarctic Islands**

143 Over the past 8.1 ka, the mean Hg accumulation rates (HgAR) at Bird Island BI10 were $31.9 \pm 18.3 \mu\text{g}$
 144 $\text{m}^{-2} \text{yr}^{-1}$ (1σ , $n = 155$, Supplementary Table S1; Fig. 2A), significantly higher than at the control sites at
 145 the Falkland Islands FIGG and mainland South Georgia POB4 ($p < 0.01$ for both). BI10 was characterized
 146 by prominent fluctuations with a maximum HgAR value of $97 \mu\text{g} \text{m}^{-2} \text{yr}^{-1}$. The mean HgAR during the
 147 oldest peat formation period at BI10 of 8.1 to 6.8 ka BP was $9.2 \pm 3.1 \mu\text{g} \text{m}^{-2} \text{yr}^{-1}$ (1σ , $n = 4$). This was
 148 followed by an approximately five-fold increase to a mean of $43.2 \pm 19.0 \mu\text{g} \text{m}^{-2} \text{yr}^{-1}$ (1σ , $n = 7$) from c.
 149 6.8 to 6.1 ka BP, and four other prominent HgAR peaks of up to a millennium in duration in more
 150 recent years; 5.2 – 3.5 ka BP, 2.7 – 2.1 ka BP, 1.4 – 1.2 ka BP and 0.5 – 0.1 ka BP, with HgAR of $48.3 \pm$
 151 18.2 (1σ , $n = 28$), 45.8 ± 12.2 (1σ , $n = 30$), 50.0 ± 21.1 (1σ , $n = 6$) and $26.7 \pm 6.1 \mu\text{g} \text{m}^{-2} \text{yr}^{-1}$ (1σ , $n = 15$),
 152 respectively (Fig. 2A).

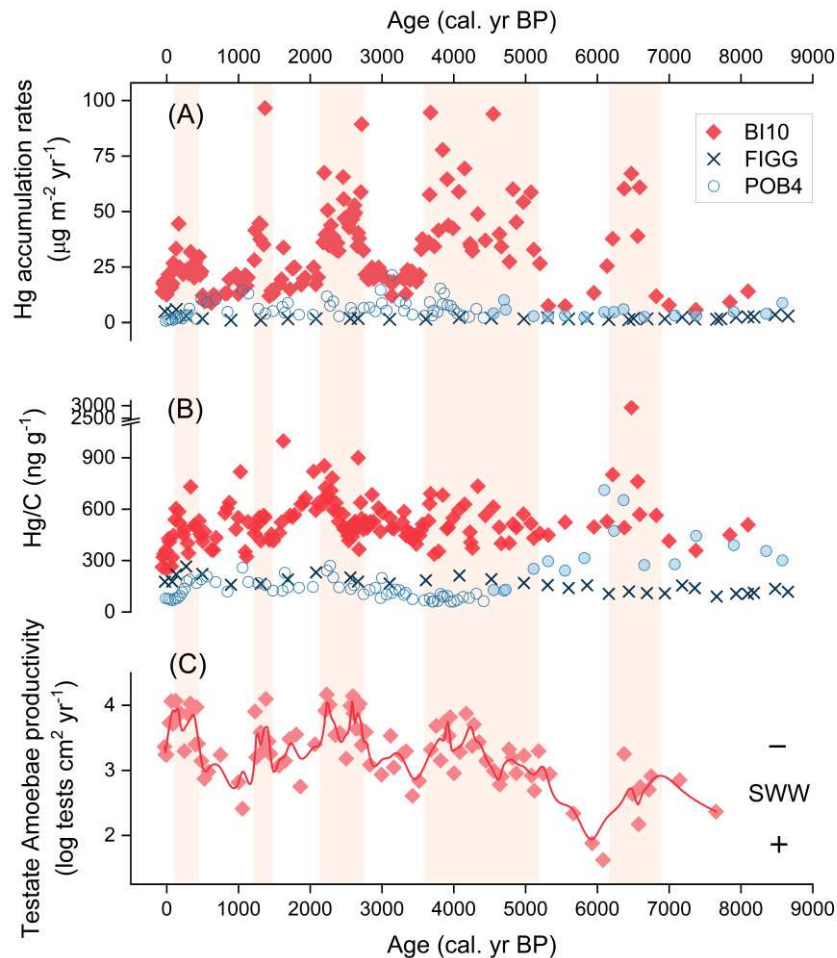
153

154 In contrast, HgAR at the control site FIGG ranged from 1.1 to $5.9 \mu\text{g} \text{m}^{-2} \text{yr}^{-1}$, with a mean of 2.2 ± 1.1
 155 $\mu\text{g} \text{m}^{-2} \text{yr}^{-1}$ (1σ , $n = 33$; Supplementary Table S2). This mean is lower than that in the mainland South
 156 Georgia POB4 profile, which was $6.0 \pm 3.9 \mu\text{g} \text{m}^{-2} \text{yr}^{-1}$ (1σ , $n = 74$, $p < 0.01$, Supplementary Table S3; Fig.
 157 2A). Both FIGG and POB4 receive Hg predominantly from the atmosphere by vegetation uptake of Hg^0
 158 and rainfall supply of Hg^{II} ³⁵. The mean HgAR at both FIGG and POB4 are comparable to global natural
 159 background levels for peat ($4.5 \pm 3.2 \mu\text{g} \text{m}^{-2} \text{yr}^{-1}$, 1σ , $n = 17$ peat cores)⁴⁸.

160

161 Holocene HgAR was significantly higher at BI10 than at FIGG and POB4, implying an additional,
 162 predominant source of Hg at the BI10 site (Fig. 2A). This was also reflected in the BI10 Hg/C profile
 163 (Fig. 2B), which normalizes Hg accumulation for changes in peat carbon accumulation. BI10 Hg/C
 164 shows a broadly increasing trend during the periods of high HgAR, suggesting excess Hg inputs
 165 compared to the FIGG and POB4 sites (Fig. 2B). BI10 Hg/C was at least three times higher than in the
 166 FIGG and POB4 peat cores (to c. 4.5 ka BP in POB4; Supplementary note 1), even though the mean
 167 percentage of carbon in the BI10 peat ($39.0 \pm 5.8 \%$, 1σ ; $n = 155$) was not significantly different from

168 that of FIGG ($43\% \pm 3.70\%$, $n = 65$, $p > 0.05$) and POB4 ($42.4 \pm 6.7\%$, $n = 59$, $p > 0.05$; Supplementary
 169 Table S1, S2, S3).
 170



171
 172 **Fig. 2:** (A) Hg accumulation rates in peat cores at Bird Island, South Georgia (BI10, diamonds), Falkland
 173 Islands (FIGG, crosses), and mainland South Georgia (POB4, peat section from 0 – 4.5 ka BP in open
 174 circles, sediment section from c. 4.5 – 9.0 ka BP in filled circles). (B) Hg/C profiles in BI10, FI, and POB4
 175 cores. (C) The intensity of Southern Westerly Winds (SWW) reconstructed from BI10 *testate amoebae*
 176 productivity that is sensitive to wind-blown sea spray (Supplementary note 2) ^{49,50}. The red line
 177 represents the data smoothed using a 3-point moving average. Orange-shaded areas highlight five
 178 periods with high HgAR linked to enhanced guano input.
 179

180 The most likely additional source of Hg at BI10 is the input of seabird guano, as this has a very high Hg
 181 content ($1,200$ to $21,600$ ng g^{-1} , dry weight, Supplementary Table S4; Supplementary note 3). Seabirds
 182 currently breeding in the BI10 catchment at Bird Island include white-chinned petrel *Procellaria*
 183 *aequinoctialis*, wandering albatross *Diomedea exulans*, northern giant petrel *Macronectes halli*,
 184 southern giant petrel *Macronectes giganteus*, Antarctic prion *Pachyptila desolata*, and brown skua
 185 *Stercorarius antarcticus*, of which the first four species are likely the main sources of guano given their
 186 large body sizes and, for white-chinned petrels, also high nesting densities. Seabird guano is known to
 187 increase Hg levels in adjacent terrestrial environments ⁵¹.
 188

189 Human activities can be excluded as an important long-term Hg source at BI10, because Bird Island
 190 was first discovered in 1775 CE ⁴¹, and apart from occasional sealing activities, was occupied
 191 intermittently by small numbers of researchers from 1957 until a small permanent research station
 192 operated year-round from 1982 onwards. Additionally, the substantial difference in HgAR between

193 BI10 and the two control sites cannot be explained by differences in plant species composition⁴⁰. All
194 these sites were influenced predominantly by an oceanic cold climate with a vegetation of graminoids,
195 dwarf shrubs, and mosses. The atmospheric Hg pool is also unlikely to be the predominant source for
196 BI10 during the mid to late Holocene because similarly elevated Hg deposition would then have been
197 expected at our control sites, POB4 and FIGG, as the atmospheric Hg pool is relatively well-mixed at
198 hemispheric scales⁵². Furthermore, the climate has been comparatively stable over the last c. 8.1 ka,
199 with no dramatic glacial-interglacial scale shifts that could substantially increase (or decrease) regional
200 atmospheric Hg deposition⁵³. Nor were there periods of very high dust deposition with substantial
201 oxidized Hg, as was the case during the last glacial period⁵³.

202

203 During periods of high Hg flux, the principal climate signal reconstructed from the BI10 peatland site
204 indicated lower wind intensities (reconstructed from *testate amoebae* productivity that is sensitive to
205 wind-blown sea spray^{49,50}, Supplementary Note 2, Fig. 2C). This suggests a potential link between high
206 guano Hg accumulation and a more favorable climate regime for nesting seabirds at Bird Island.
207 Additionally, this link indicates that wind-regulated rainfall may not play a significant role in guano
208 deposition at the peatland site over the long term (i.e., catchment hydrological influence). Lower wind
209 intensity is accompanied by lower humidity and rainfall³⁴, which could have led to lower guano runoff
210 and Hg deposition in BI10 peat, contrary to the observations. Next, we discuss how Hg stable isotopes
211 can fingerprint seabird guano as the dominant source of Hg in BI10.

212

213 Seabird guano Hg contribution constrained by Hg stable isotopes

214

215 Mercury has seven stable isotopes with masses ranging from ¹⁹⁶Hg to ²⁰⁴Hg that can undergo mixing
216 or fractionation via transformation processes⁵⁴. Unlike $\delta^{202}\text{Hg}$, which represents a typical mass-
217 dependent fractionation (MDF) of Hg isotopes, the odd-mass Hg isotopes can undergo mass-
218 independent fractionation (MIF, $\Delta^{199}\text{Hg}$ or $\Delta^{201}\text{Hg}$) in specific processes, such as photochemical
219 reactions⁵⁴. In contemporary seabird guano collected at Bird Island, $\Delta^{199}\text{Hg}$ was $1.32 \pm 0.05\text{‰}$ (1σ , n
220 $= 5$, Supplementary table S4), comparable with penguin guano from the Antarctic Peninsula ($0.96 \pm$
221 0.03‰ , 1σ , $n = 2$)²⁷. Guano Hg acquires its distinct positive $\Delta^{199}\text{Hg}$ from the marine methylmercury
222 (MeHg, organic form of Hg) when marine MeHg is partly degraded by sunlight in ocean surface waters
223⁵⁵. The pool of residual marine MeHg with positive $\Delta^{199}\text{Hg}$ subsequently bioaccumulates and
224 biomagnifies in the marine foodweb, leaving its signature in guano, whose Hg is composed of up to
225 100% of MeHg³³. Guano Hg inputs to peat, therefore, carry distinctly more positive $\Delta^{199}\text{Hg}$ than
226 atmospheric Hg inputs to peat ($\text{Hg}^0 \Delta^{199}\text{Hg} = -0.28 \pm 0.05\text{‰}$, 1σ , $n = 23$; and $\text{Hg}^{\text{II}} \Delta^{199}\text{Hg} = 0.21 \pm 0.42\text{‰}$,
227 1σ , $n = 21$)³⁴.

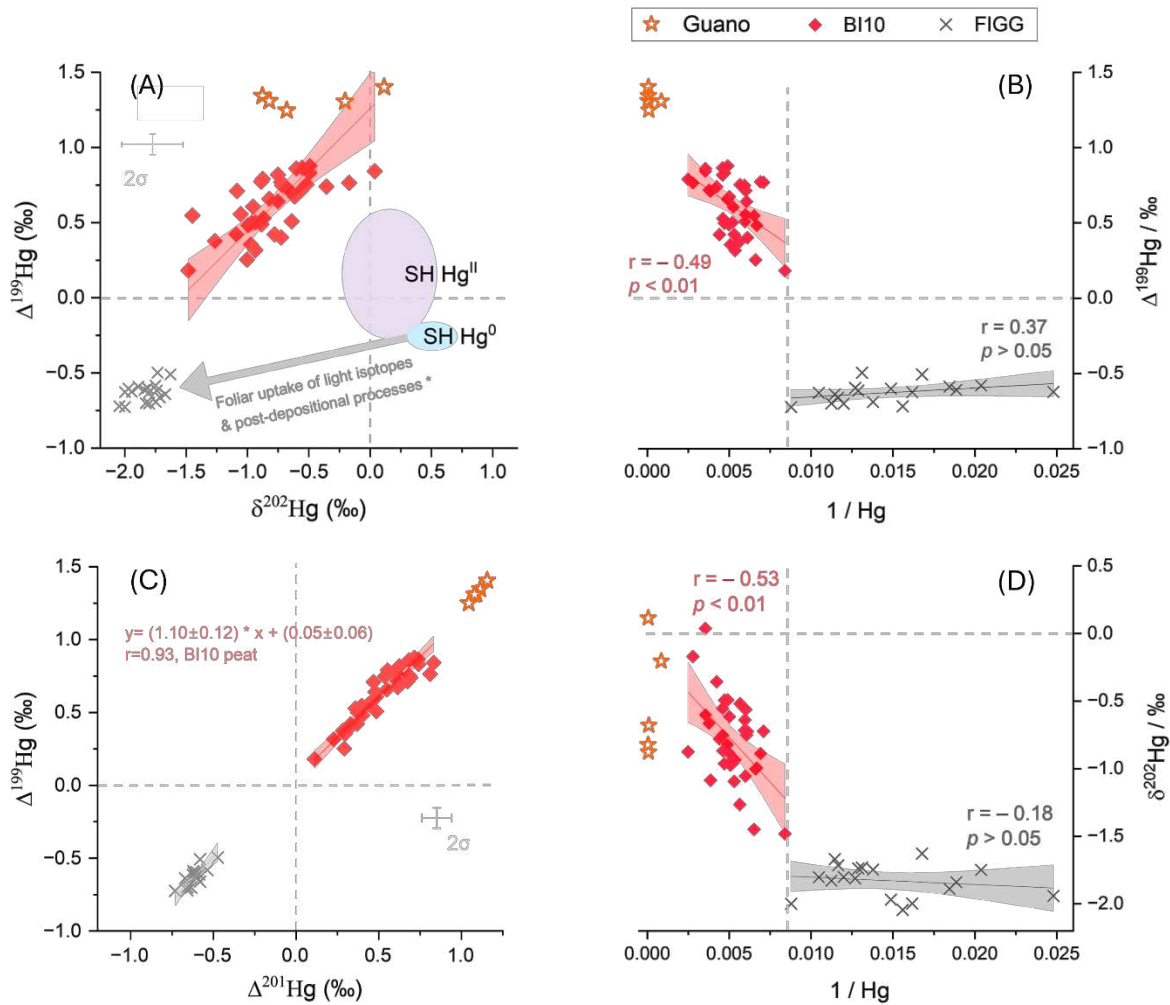
228

229 Mean $\Delta^{199}\text{Hg}$ at BI10 was $0.61 \pm 0.19\text{‰}$ (1σ , $n = 36$, Fig. 3A), and showed a significant negative
230 relationship with $1/\text{Hg}$ ($r = -0.49$, $p < 0.01$, Fig. 3B). This indicates that higher $\Delta^{199}\text{Hg}$ is concomitant
231 with higher Hg concentrations at BI10, which is in line with guano $\Delta^{199}\text{Hg}$ and Hg concentration
232 signatures. In contrast, the $\Delta^{199}\text{Hg}$ at FIGG was negative overall, with a mean of $-0.63 \pm 0.06 \text{‰}$ (1σ , n
233 $= 18$) and no significant relationship with $1/\text{Hg}$ ($p > 0.05$). The binary source mixing diagram, Fig. 3B,
234 showing linearized $1/\text{Hg}$ vs $\Delta^{199}\text{Hg}$, indicates that the high Hg concentrations in BI10 can be explained
235 by simple source mixing of guano Hg inputs and atmospheric Hg (manifested as predominant source
236 at FIGG). The $\Delta^{199}\text{Hg}$ determined in peatlands worldwide without identified avian influences^{34,37,56,57}
237 is generally negative due to the inherently negative $\Delta^{199}\text{Hg}$ (-0.28‰) of atmospheric Hg^0 that
238 accumulates in peat. Post-depositional negative shifts in peat soil $\Delta^{199}\text{Hg}$ occur due to predominant
239 sulfur-ligand bound peat Hg^{II} photoreduction⁵⁸ or dark abiotic reduction⁵⁹, which leaves more
240 negative $\Delta^{199}\text{Hg}$ in the peat residue, as observed for FIGG (Fig. 3A; Supplementary note 4). These
241 reduction processes, if they occur, will not cause such a positive $\Delta^{199}\text{Hg}$ as recorded at the BI10 site

242 (0.61 ± 0.19‰). Furthermore, as evidenced by the slope of $\Delta^{199}\text{Hg}/\Delta^{201}\text{Hg}$ as a process indicator, the
243 BI10 peat signature (1.10 ± 0.12, 1 σ , Fig. 3C) is comparable to that of MeHg in marine biota (~1.20)
244 ^{60,61}. Overall, contrasting values of $\Delta^{199}\text{Hg}$ between BI10 and peatlands largely free from seabird colony
245 influence confirm the influence of guano input to the BI10 site.

246
247 Similar to $\Delta^{199}\text{Hg}$, $\delta^{202}\text{Hg}$ in BI10 ($-0.79 \pm 0.31\text{‰}$, 1 σ , n = 36, Fig. 3D), was also significantly higher than
248 in FIGG, which ranged from -2.04‰ to -1.63‰ ($p < 0.01$). Fractionation of $\delta^{202}\text{Hg}$ occurs during all
249 physical, chemical, and biological processes ⁵⁴. At our reference site, the FIGG peat $\delta^{202}\text{Hg}$ values show
250 a mean shift of -2.25‰ from the dominant atmospheric Hg^0 sources to peat ($\text{Hg}^0 \delta^{202}\text{Hg} = 0.51 \pm$
251 0.16‰ , 1 σ , n = 23) ³⁴. Low $\delta^{202}\text{Hg}$ in FIGG is a result of preferential foliar uptake of light Hg isotopes
252 from the atmospheric gaseous Hg^0 pool ³⁵ (Fig. 3A), which is in good agreement with global peatlands
253 ^{34,37,56,57}. Significantly higher $\delta^{202}\text{Hg}$ in BI10 than FIGG is most likely due to the input of guano with a
254 high Hg concentration and a mean $\delta^{202}\text{Hg}$ value of $-0.49 \pm 0.39\text{‰}$ (1 σ , n = 5). This is further evidenced
255 in the significant negative correlation between BI10 $\delta^{202}\text{Hg}$ and 1/Hg ($r = -0.53$, $p < 0.01$, Fig. 3D).
256 Additionally, BI10 $\Delta^{199}\text{Hg}$ and $\delta^{202}\text{Hg}$ were positively and significantly correlated ($r = 0.67$, $p < 0.01$, Fig.
257 3A), implying that the variability of these two isotope signatures in peat is more driven by Hg sources,
258 rather than post-depositional processes. The important Hg post-depositional processes, such as
259 sulfur-ligand bound peat Hg^{II} photoreduction or dark abiotic reduction ^{58,59,62}, generally lead to more
260 negative $\Delta^{199}\text{Hg}$ and more positive $\delta^{202}\text{Hg}$ signatures in peat residue, which is contrary to their positive
261 correlation in BI10. Taken together, the peat $\delta^{202}\text{Hg}$ signature further confirms a dominant guano
262 contribution to the BI10 site.

263
264



265

266 **Fig. 3:** (A) $\Delta^{199}\text{Hg}$ vs $\delta^{202}\text{Hg}$, (B) $\Delta^{199}\text{Hg}$ vs $1/\text{Hg}$, (C) $\Delta^{199}\text{Hg}$ vs $\Delta^{201}\text{Hg}$, and (D) $\delta^{202}\text{Hg}$ vs $1/\text{Hg}$ in BI10 (red
 267 solid diamonds) in comparison to FIGG peat profile (grey crosses) and Bird Island guano (orange open
 268 stars). Grey arrow in (A) indicates preferential foliar uptake of light isotopes from the Southern
 269 Hemisphere atmospheric Hg^0 pool (SH Hg^0 , blue filled ellipse), and peat Hg isotope signatures after
 270 post-depositional processes on deposited Hg^0 and rainfall Hg^{II} (SH Hg^{II} , purple filled ellipse)³⁴. The
 271 vertical dashed lines in (B) and (D) operationally separate $1/\text{Hg}$ above 0.0087 (FIGG data) and below
 272 (BI10 data). The red and grey lines in A-D indicate the linear fit to data from BI10 and FIGG,
 273 respectively, and the shaded areas indicate the 95% confidence band.

274

275 Guano nutrient-fueled Hg sequestration by peat vegetation

276

277 In addition to Hg, guano contributes a substantial amount of nutrients (e.g., N, P) to peatland
 278 ecosystems, promoting vegetation growth⁶³. This could be the reason why during c. 8.1 – 0.2 ka BP,
 279 carbon accumulation rates in BI10 were $62 \pm 33 \text{ g C m}^{-2} \text{ yr}^{-1}$ (1σ , $n = 143$, below water table level),
 280 which is 4 times higher than at the FIGG site ($12 \pm 4 \text{ g C m}^{-2} \text{ yr}^{-1}$, 1σ , $n = 54$; Supplementary Fig. S4;
 281 Supplementary Table S1, S2)⁶⁴. Without significant avian influence via guano fertilization, long-term
 282 carbon accumulation rates on sub-Antarctic Islands are generally low due to the cold climate⁶⁵, with
 283 multi-millennial mean values typically below $20 \text{ g C m}^{-2} \text{ yr}^{-1}$ ⁶⁶. Despite being affected by fire activities
 284⁶⁴, FIGG carbon accumulation is comparable to the accumulation rates in some Falkland Islands peat
 285 profiles spanning a similar timescale (e.g., mean $19 \text{ g C m}^{-2} \text{ yr}^{-1}$ from Whalebone Cove since c. 8.0 ka
 286 BP, with $18.73 - 19.34 \text{ g C m}^{-2} \text{ yr}^{-1}$ for 5th to 95th percentile)⁶⁶. Peat carbon accumulation rates result from

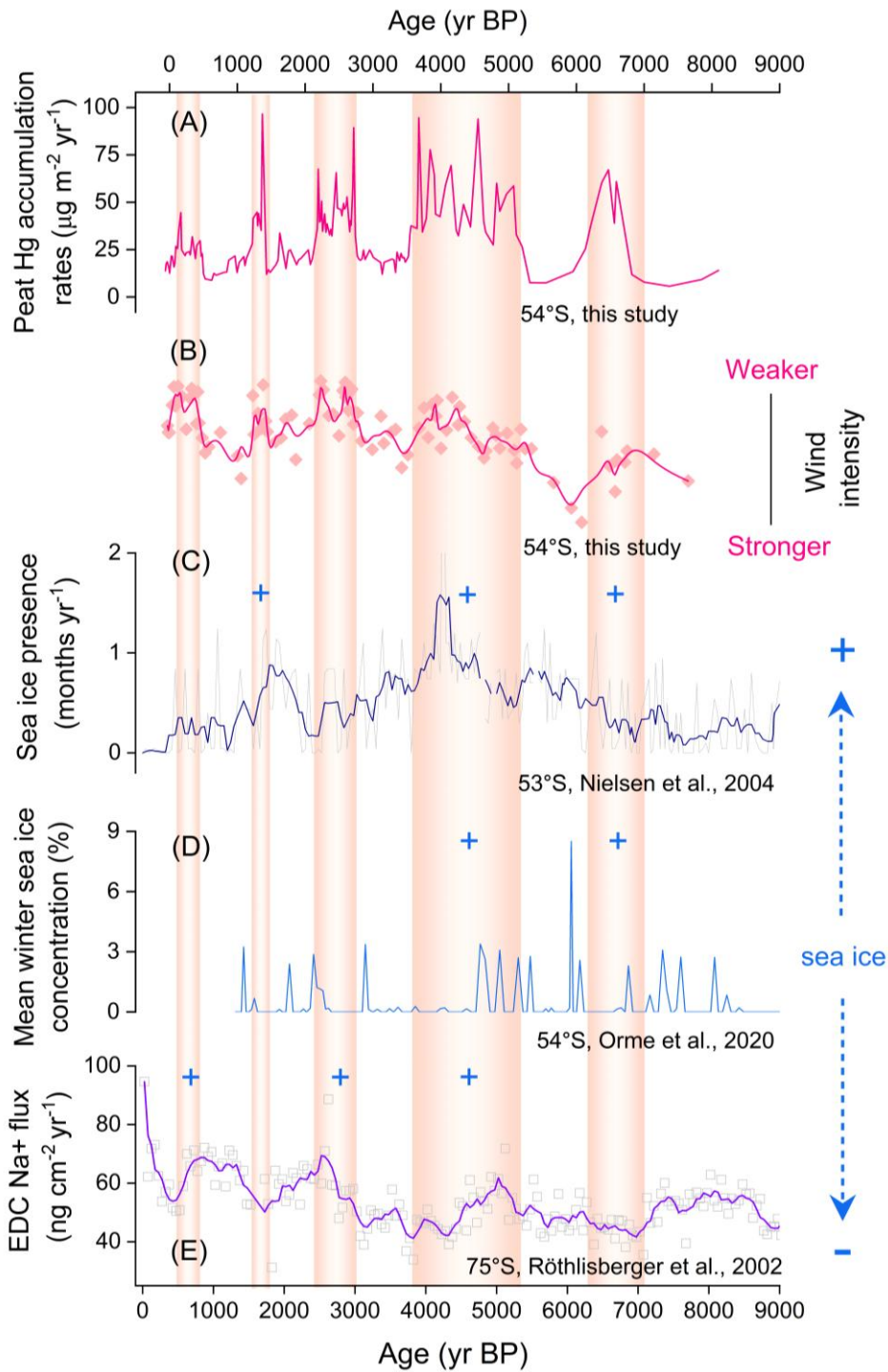
287 the mass balance between primary production and decomposition loss. Significantly higher carbon
288 accumulation rates at BI10 compared to FIGG could be explained by enhanced primary productivity
289 fueled by guano nutrient input, instead of a lower decomposition rate at BI10. Although nutrient
290 inputs through guano can also facilitate the rates of peat decomposition⁶⁶ due to enhanced microbial
291 activities, nutrient-fueled primary productivity at BI10 appears to outweigh higher decomposition
292 rates, ultimately leading to high carbon accumulation rates at the BI10 site. This phenomenon has also
293 been documented in Beauchene Island, the southernmost of the Falkland Islands, where the long-
294 term apparent carbon accumulation rates are also very high ($139 \text{ g C m}^{-2} \text{ yr}^{-1}$)^{66,67}. N and P fluxes from
295 seabird populations globally are estimated to be 591 Gg N yr^{-1} and 99 Gg P yr^{-1} , with the highest input
296 in Antarctica and Southern Ocean regions⁶⁸. Overall, guano nutrient input promotes peat vegetation
297 growth and carbon sequestration. Enhanced peat vegetation growth presumably leads to increased
298 Hg^0 uptake, hence higher HgAR.

299
300 Increased Hg^0 uptake can be examined by the relatively conservative Hg source tracer, even-Hg MIF
301 (represented by $\Delta^{200}\text{Hg}$), although it generally has very small variations among sources^{54,69}. During
302 high HgAR periods, BI10 peat $\Delta^{200}\text{Hg}$ is $-0.04 \pm 0.03 \text{ ‰}$ (1σ , $n = 20$, Supplementary Fig. S4). These BI10
303 periods were characterized by lower $\Delta^{200}\text{Hg}$ values than BI guano $\Delta^{200}\text{Hg}$ signatures ($0.01 \pm 0.01 \text{ ‰}$, n
304 $= 5$). In contrast, BI10 $\Delta^{200}\text{Hg}$ values appear to be more commonly associated with atmospheric Hg^0
305 composition ($-0.06 \pm 0.02 \text{ ‰}$, 1σ , $n = 23$)³⁴, indicating higher atmospheric Hg^0 sequestration by peat
306 vegetation. Evidences from peat carbon accumulation rates and $\Delta^{200}\text{Hg}$ suggest two important sources
307 of Hg to the BI10 record, particularly during peak HgAR phases (Fig. 4A): elevated Hg directly from
308 guano, and enhanced plant uptake of Hg^0 associated with greater primary production fueled by guano
309 nutrients.

310
311 Besides the peak HgAR phases in the BI10 profile, there are five periods with lower HgAR (i.e. c. 8.1 –
312 6.8, 6.1 – 5.2, 3.5 – 2.7, 2.1 – 1.4, 1.2 – 0.5 ka BP, Fig. 4A). A likely explanation for the periods of lower
313 Hg accumulation in BI10 is less guano input linked to lower seabird breeding densities in the peatland
314 catchment. In contrast, photochemical Hg loss from peatlands, which is identified as the main Hg loss
315 pathway⁵⁷, is not a primary cause for low Hg accumulation periods at BI10. Because these periods
316 reflect higher wind intensity (Fig. 4B) and accompanying increased humidity and cloud cover, which
317 are associated with lower insolation in the study site.

318 319 **Seabird establishment and population dynamics**

320
321 High peat HgAR implies more guano input, which we interpret as higher seabird densities in the
322 catchment of BI10 (and vice versa). The peatland formation at BI10 was initiated c. 8.1 ka, likely
323 associated with gradual warming during the early Holocene in the Southern Ocean region ($45\text{--}60^\circ\text{S}$)
324⁷⁰. At the onset of peat initiation, BI10 was characterized by guano-like positive $\Delta^{199}\text{Hg}$ and high Hg/C
325 (Supplementary Fig. S4). This suggests the first colonization of Bird Island by seabirds was around 8.1
326 ka, but possibly before, and associated with the retreat of glaciers and perennial snow cover. The first
327 period of sustained growth of the seabird colony at BI10 was during c. 6.8 – 6.1 ka, reflected in a
328 pronounced increase in HgAR (Fig. 4A). This is in line with the timing of colonization of Antarctic Ardley
329 Island (South Shetland Islands) by penguins¹⁹, but pre-dates other sub-fossil and geochemical
330 evidence of occupation of the eastern coast of the sub-Antarctic Falkland Islands by at least 1000 years
331¹⁷.



332
 333
 334
 335
 336
 337
 338
 339
 340
 341
 342
 343

Fig. 4: (A) Hg accumulation rates at BI10 (HgAR, 54°S, this study). (B) SWW intensity reconstructed by *testate amoebae* productivity at the BI10 site^{49,50}. (C) Sea-ice presence from the Antarctic Polar Front in the east Atlantic Ocean (53°S, Fig. 1A)⁴⁵. The dark blue line depicts the results of 3-point smoothing. (D) Mean winter (September) sea-ice concentrations for core COR1GC (54°S, Fig. 1A)⁴⁶. The modern winter sea-ice concentration is marked as 0 as the sea-ice limit is at 59°S. (E) DOME C sea-salt sodium as a proxy for sea salt (75°S, Fig. 1A)⁴⁷. Sea-salt concentrations are thought to be influenced by the sea-ice extent and wind speed in the potential source region, as well as the transport from there to the ice core site. The purple line depicts the results of 3-point smoothing. Blue crosses indicate enhanced sea-ice cover. Orange-shaded areas highlight five periods with high Hg flux linked to enhanced guano input.

344 Including the colonization at c. 6.8 – 6.1 ka, there were five periods of high Hg fluxes, associated with
345 locally higher seabird abundance (the others were at c. 5.2 – 3.5, 2.7 – 2.1, 1.4 – 1.2, and 0.5 – 0.1 ka;
346 Fig. 4). All five periods are aligned with periods of weaker Southern Westerly Wind (SWW) intensity
347 reconstructed from *testate amoebae* productivity (Figs. 4A, 4B). Wind regimes affect seabird energy
348 budgets and flight costs, influencing foraging trip durations, chick provisioning rates, breeding success
349 and hence population dynamics⁷¹. Weaker SWW, therefore, potentially promoted seabird breeding
350 in the BI10 catchment areas. Conversely, during sustained periods of high winds, the slopes above
351 BI10 became less suitable for nesting because of increased risk of crash landing, flooding, thermal
352 exposure or, in surface-nesting species, of adults or chicks being blown off their nests, any of which
353 can lead to breeding failure⁷¹.

354

355 The main driver of population growth rates in seabirds in natural situations is the availability of prey
356⁷². The four seabird species most likely to be the sources of most of the guano at BI10 are the white-
357 chinned petrel, wandering albatross, northern giant petrel and southern giant petrel, which exploit
358 prey over very large areas^{73–76}. These areas include the Patagonian Shelf and slope, Scotia Arc
359 (including the South Georgia, South Sandwich and South Orkney Islands) and the southern water mass
360 boundary of the Antarctic Circumpolar Current, the Subtropical Front, and the Subantarctic Front (Fig.
361 1B). Although these species have diverse diets that may include fish, squid, crustaceans and carrion,
362 they all exploit the seasonal sea-ice zone at some stage in the breeding season, typically with a lag of
363 several weeks presumably corresponding to the time taken for the spring plankton bloom to transfer
364 energy to mid-trophic-level prey such as squid, fish or zooplankton⁷⁶. For white-chinned petrels and
365 giant petrels, a major component of their diets during chick rearing is Antarctic krill^{14,77}; this feeds on
366 sea-ice algae and is a key species within Southern Ocean food webs^{78–80}.

367

368 All five elevated Hg flux phases in BI10 peat occurred during periods of decreased SWW (Fig. 4B) and
369 increased sea-ice extent in the Southern Ocean (Fig. 4C–E), so it seems reasonable to conclude that
370 climate and environmental conditions in the Southern Ocean 5000 years ago favored seabirds
371 breeding at Bird Island and elsewhere at South Georgia. Between c. 5 – 3.5 ka, seabird densities at
372 BI10 were presumably high for a period of ~1500 years when sea ice extended to as far north as the
373 Antarctic Polar Front (Fig. 4C–E). At this time, higher prey abundance in the Southern Ocean possibly
374 contributed to the establishment of seabirds or seals breeding at Surf Bay site on the east coast of the
375 Falkland Islands, as evidenced by marine-derived nutrients from guano facilitating tussac grass
376 establishment and increased peat-forming plant productivity, and increased peat accumulation¹⁷.

377

378 **Implications**

379 South Georgia is a globally important breeding site for seabirds, including several threatened species.
380 Currently, knowledge of seabird population response to climate change and anthropogenic pressures
381 is limited largely to the period since the 1950s, i.e., recent, decadal timescales. By extending the record
382 of population change back thousands of years, our study has advanced our understanding of how
383 seabird populations have varied on centennial to millennial timescales and how they respond to long-
384 term natural variability in climate and marine ecosystems. This is particularly important because
385 populations of pelagic seabirds have declined dramatically since the 1950s, which must be interpreted
386 both in the context of direct anthropogenic impacts, and indirect anthropogenic impacts on climate
387^{1,2}. The former includes resource exploitation (fisheries)⁸¹, pollution (e.g., plastics)⁸², and ecosystem
388 impacts of invasive species (predation by mice and rats)⁸³, while the latter includes intensification and
389 southward displacement of the SWW⁸⁴ and retreat of sea ice in the South Atlantic sector of the
390 Southern Ocean⁸⁵. For the climate impacts, this study provides a long-term perspective on which to
391 base more accurate predictions of future changes in seabird populations. These include impacts on
392 breeding success on individual islands as the core belt of the SWW intensifies and moves southward,

393 and on prey availability in the foraging zone as the sea ice retreats.

394 To summarize, our study has shown that: 1) Hg can be used as a reliable tracer of guano influx into
395 peatlands because Hg cannot be recycled by peat vegetation as an essential element; 2) seabirds on
396 Bird Island created substantial volumes of Hg-rich guano, with distinct Hg isotope signatures that were
397 archived in peat, providing a long-term record of changes in nesting densities; 3) The Bird Island BI10
398 site (colony) experienced five Hg-reconstructed population maxima from the mid to late Holocene, all
399 of which correspond with lower prevailing westerly wind intensity over the catchment, that likely
400 resulted in more favorable foraging and breeding conditions in the region.

401

402

403 **Methods**

404 **Study sites and sampling**

405 **Bird Island**

406 Situated south of the Antarctic Polar Front (Fig. 1A), Bird Island is exposed directly to Antarctic storms
407 from the southwest. Gale-force winds can occur all year round. It is cold, cloudy, and wet all year
408 round. The annual temperature is 1.2 °C, and the annual rainfall is ~850 mm with an average humidity
409 of 84%⁸⁶. Temperatures vary from -10°C to 10°C, ~0°C in winter and ~4°C in summer, which is
410 characterized by damp, misty, low cloud conditions⁸⁶. In winter, the snow cover lasts from July to
411 October, but there is no permanent ice cap, ice, or glaciers on the island, in contrast to mainland South
412 Georgia.

413 The peat coring site, BI10 (54°01'04.9"S, 38°04'13.7"W) is from a valley floor mire located between
414 the headland at Morris Point and Gony Ridge, surrounded by slopes that are primarily vegetated with
415 tussock grass (*Poa flabellata*) with mosses, including *Chorisodontium aciphyllum* and *Polytrichum*
416 *alpestre*. The site is approximately 30 m above sea level on the western side of the island and therefore
417 directly exposed to the westerly winds. It receives water largely from surface drainage, with a high
418 water table sustained through gravitational lateral seepage from adjacent slopes⁴². The sampled
419 valley mire can, therefore, record guano input through runoff from the surrounding catchment where
420 there are nesting seabirds. The water table level is at 10 – 15 cm below the peat surface.

421 A 5 m-long peat sequence was collected from the BI10 site in Feb 2017 using a 50 × 6 cm Russian
422 corer. Peat cores were described and wrapped in plastic film before placement in PVC tubes and
423 transported to the British Antarctic Survey for frozen storage. Five samples of fresh guano from
424 albatrosses were also collected on Bird Island and stored frozen in plastic tubes.

425

426 **South Georgia**

427

428 Located approximately 1,400 km south-east of the Falkland Islands, South Georgia lies between
429 latitudes 54°S and 55°S, and longitudes 36°W and 38°W (Fig. 1B). Its climate is typical of the maritime
430 subantarctic, with annual mean temperatures of 2.0°C, precipitation of 1,590 mm per year recorded
431 at the research station, King Edward Point⁸⁷. Temperatures range from -15°C to +20°C (with higher
432 temperatures on the lee side of the mountains enhanced by foehn winds)⁸⁷, with snow covering from
433 May to October. Situated in the northwest of South Georgia, Prince Olav Bog (POB4,
434 54°04'06"S, 37°06'40"W) is a Sphagnum-dominated peat bog with only 1-2 pairs of giant petrels
435 nesting in the catchment (Fig. 1). *Sphagnum fimbriatum* forms dry hummock-like patches, surrounded

436 by wet hollows that are dominated by monocots and brown mosses. A 3.6 m–long peat profile was
437 collected at one of the Sphagnum patches in 2008 using a 50 × 8 cm long Russian peat corer.

438

439 **Falkland Islands**

440 The Falkland Islands are located between 51°S and 52°30'S and 57° 45'W and 61°30'W. They consist
441 of two large islands (East Falkland, about 6700 km², and West Falkland, about 5300 km²), with
442 approximately 700 smaller islands. The archipelago is about 700 km north-east of Cape Horn and 500
443 km east of the nearest part of the South American continent (Fig. 1). The coring site is ~12 km east of
444 the settlement of Goose Green (FIGG) in an open basin, lying slightly lower than the surrounding hills.
445 The climate is cool maritime, with annual mean temperatures of ~6°C, precipitation of ~600 mm per
446 year, and a mean wind speed of ~30 km h⁻¹ ⁸⁸.

447 The coring site, FIGG, is characterized by a typical acid 'whitegrass' (*Cotaderia egmontia*) peatland,
448 with *Blechnum penna-marina*, *Baccharis magellanica*, *Empetrum rubrum*, *Oreobolus obtusangulus*,
449 *Gaultheria pumila* and *Myrteola nummularia*. This coring site is also not currently a nesting ground for
450 seabirds. A 3.6 m-long peat sequence was collected in 2022 using a stainless-steel box of 10 × 10 cm
451 for the top 50 cm of the peat profile, with the remainder sampled using a Russian peat corer with a
452 50 × 8 cm chamber.

453 **Peat subsampling**

454 Cores were frozen and subsequently sliced at ~1 cm resolution for the whole core. Each new slice was
455 cleaned with MilliQ water, edges removed, and subsampled for further analysis following established
456 protocols ⁸⁹. The dimension of the largest subsample of each slice was measured using a Vernier
457 caliper to obtain the volume for calculating the dry bulk density and to estimate the cut loss between
458 each slice. Subsequently, the largest sub-samples from BI10 and POB4 were dried for geochemical
459 analysis using the freeze-dryers at the University of Toulouse, while those from FIGG were oven-dried
460 at 40 – 50°C at the University of Aberdeen.

461

462 **Radiocarbon dating and age models**

463

464 In total, ×14 plant macrofossil samples from Bird Island BI10, ×8 from South Georgia POB4, and ×9
465 from the Falkland Islands FIGG, were selected for radiocarbon analyses following established protocols
466 ⁹⁰. All the selected samples were prepared and analyzed for radiocarbon analysis at the University of
467 Aberdeen and the ¹⁴CHRONO Centre at Queen's University Belfast, respectively. The age models for
468 BI10 peat profiles, POB4 and FIGG were generated from ¹⁴C results using the Bacon model (calibration
469 curve SH Cal20) with the 'rbacon' package in R software (<https://CRAN.R-project.org/package=rbacon>)
470 ⁹¹. Details on the dated material and radiocarbon ages from BI10 and FIGG are detailed in refs ^{50,64},
471 while POB4 is shown in the Supplementary Table S5.

472 BI10 has a chronology of 8.1 ka (Supplementary Fig. S3). The entire POB4 core is 380-cm long with a
473 chronology of 8.5 ka constrained by eight radiocarbon dates (Supplementary Fig. S2). This Bog was
474 formed from a dried lake approximately c. 4.5 ka ago, with a sediment section during c. 8.5-4.5 ka BP
475 followed by a peat section from c. 4.5 ka BP onwards (Supplementary note 1).

476 **Carbon measurements**

477 Carbon content in BI10 and POB4 was estimated from Loss of Ignition (LOI) at 550°C, with carbon
478 content estimated as approximately half of LOI ⁹². Dried peat samples are combusted to ash and
479 carbon dioxide at 550°C ⁹³. The LOI is then calculated using the following equations:

480 $LOI550 = ((DW105 - DW550) / DW) * 100$ (1)

481 Carbon content in FIGG was analyzed using a Flash Combustion Elemental Analyser (CE Instruments
482 NA 2500 Flash Combustion EA) ⁶⁴.

483 **Hg concentration measurements and Hg accumulation rate calculation**

484 Dried peat samples from BI10, POB4 and, FIGG were analyzed for total Hg (THg) concentration on a
485 combustion cold vapor atomic absorption spectrometer (CV-AAS, Milestone DMA-80) at the
486 University of Bern, Switzerland. The analytical performance of the DMA-80 was assessed by multiple
487 measurements on reference material, NIST 1515 (Apple leaves). Results were not statistically different
488 from the certified values, with Hg concentrations of $43.3 \pm 2.1 \text{ ng g}^{-1}$ (1σ , $n = 78$, certified
489 $43.2 \pm 2.3 \text{ ng g}^{-1}$) for NIST 1515.

490
491 Hg flux ($\mu\text{g m}^{-2} \text{ yr}^{-1}$, Eq. 2) in sample i was obtained by Hg concentration (ng g^{-1}), density (g cm^{-3}),
492 thickness (cm), and age interval (yr).

493
494 $\text{Hg flux} = \text{Hg concentration} \times \text{density} \times \text{thickness} / \text{age interval}$ (2)

495
496 **Hg isotope measurements**

497
498 Due to sample availability, only BI guano, BI10 peat, and FIGG peat were extracted for Hg isotope
499 analysis using a combustion method adapted from Enrico et al. ⁹⁴. Hg released from the combustion
500 procedure was collected with 40% inverse *aqua regia* solutions. Following extraction, the Hg stable
501 isotope compositions of guano (5 samples) and peat samples from Bird Island (36) and Falkland Islands
502 (18) were determined from 20% (v/v, diluted from 40%) inverse *aqua regia* solutions using cold-vapor
503 multi-collector inductively coupled mass spectrometry (CV-MC-ICP-MS, Neptune Plus, University of
504 Bern). Sample isotopic ratios were corrected for mass bias by sample-standard bracketing using NIST
505 3133 ⁹⁵. Results are reported as δ -values in per mil (‰) representing Hg mass dependent fractionation
506 by reference to NIST 3133 (Eq. 3).

507
508 $\delta^{XXX}\text{Hg} = \left\{ \frac{(^{XXX}\text{Hg}/^{198}\text{Hg})_{\text{sample}}}{(^{XXX}\text{Hg}/^{198}\text{Hg})_{\text{NIST3133}}} - 1 \right\} \times 1000$ (3)

509
510 MIF is calculated based on the deviations of δ -values from the theoretical MDF (Eq. 4).

511
512 $\Delta^{XXX}\text{Hg} = \delta^{XXX}\text{Hg} - \beta \times \delta^{202}\text{Hg}$ (4)

513
514 where XXX stands for 199, 200, 201 and 204. Symbol β is 0.2520, 0.5024, 0.7520, and 1.493
515 for ¹⁹⁹Hg, ²⁰⁰Hg, ²⁰¹Hg, and ²⁰⁴Hg, respectively.

516
517 The quality control of Hg isotope measurements is assessed by analyzing Almaden, ETH-Fluka and
518 procedural standards (Apple leaves, NIST 1515, $n = 35$, Supplementary Table S6). Almaden showed
519 $\delta^{202}\text{Hg}$ and $\Delta^{199}\text{Hg}$ of $-0.56 \pm 0.13\text{‰}$ and $-0.03 \pm 0.07\text{‰}$ (2σ , $n = 70$), respectively. ETH-Fluka displayed
520 $\delta^{202}\text{Hg}$ and $\Delta^{199}\text{Hg}$ of $-1.47 \pm 0.16\text{‰}$ and $0.08 \pm 0.07\text{‰}$ (2σ , $n = 9$), respectively. Hg isotopic signatures
521 in procedural standards are reported for $\delta^{202}\text{Hg}$ (maximum $2\sigma = 0.25\text{‰}$), $\Delta^{199}\text{Hg}$ (maximum
522 $2\sigma = 0.07\text{‰}$), $\Delta^{200}\text{Hg}$ (maximum $2\sigma = 0.05\text{‰}$), $\Delta^{201}\text{Hg}$ (maximum $2\sigma = 0.09\text{‰}$) and $\Delta^{204}\text{Hg}$ (maximum
523 $2\sigma = 0.17\text{‰}$). Hg isotope signatures of all three standards are comparable to other published Hg
524 isotope data ^{57,96,97} (Supplementary Table S6).

525

526 **Author Contributions:**

527

528 C.L. designed the project and acquired funding. S.J.R., M.G., A.M., K.B., N.B., C.J., D.H. offered great
529 mentorship. S.J.R., R.P., D.Ma., C.v.S., T.T., D.Mu., A.W., A.G-S., D.H. carried out field work. C.L., S.J.R.,
530 M.W., M.E., J.S., F.V., N.V.P., S.O., N.B., E.A., A. C-H. prepared/performed lab work and data analysis.
531 C.L. wrote the original draft. S.J.R., M.G., A.M., M.W., R.P., M.E., K.B., U.S., D.M., C.S., T.T., A.W., A-G-
532 S., J.S., F.V., N.V.P., P.B., O.M., S.O., N.B., T.F., E.A., A. C-H., P.Z., C.J., K.S., S.Y.K., D.W., R.B., L.S., D.H.
533 contributed to the discussion, interpretations, and commented on the manuscript.

534

535 **Acknowledgements**

536 This study is supported by a Swiss National Science Foundation SPF grant to C.L. (TMPFP2_210183).
537 We are very grateful to Manuela Fehr at ETH Zurich, and Christine Alewell and Judith Kobler from the
538 University of Basel, for lending their lab equipment for Hg isotope analysis. We would like to thank
539 Qasid Ahmad for his support with the cup configuration on MC-ICPMS. The MC-ICP-MS at the Institute
540 of Geological Sciences, University of Bern, used in this study was acquired within the framework of
541 the NCCR project PlanetS (grant nr. 51NF40-141881). The study is a contribution to the British
542 Antarctic Survey Polar Science for a Sustainable Planet science strategy funded by the Natural
543 Environment Research Council. A.G-S. and A.W.'s field work in BI10 was part of the "Late Quaternary
544 changes in the Westerly Winds over the Southern Ocean; the record in sub-Antarctic coastal
545 peatlands" project supported by the British Antarctic Survey (CASS126). D.Ma., C.v.S. and T.T.'s
546 fieldwork was supported by The Leverhulme Trust (grant number RPG-2020-156).

547

548

549 **References:**

- 550 1. Paleczny, M., Hammill, E., Karpouzi, V. & Pauly, D. Population Trend of the World's Monitored Seabirds,
551 1950-2010. *PLOS ONE* **10**, e0129342 (2015).
- 552 2. Phillips, R. A., Fort, J. & Dias, M. P. Conservation status and overview of threats to seabirds. in *Conservation*
553 *of Marine Birds* 33–56 (Elsevier, 2023). doi:10.1016/B978-0-323-88539-3.00015-7.
- 554 3. Whelan, C. J., Wenny, D. G. & Marquis, R. J. Ecosystem Services Provided by Birds. *Ann. N. Y. Acad. Sci.* **1134**,
555 25–60 (2008).
- 556 4. Piatt, I. & Sydeman, W. Seabirds as indicators of marine ecosystems. *Mar. Ecol. Prog. Ser.* **352**, 199–204
557 (2007).
- 558 5. Pakhomov, E. A. & McQuaid, C. D. Distribution of surface zooplankton and seabirds across the Southern
559 Ocean. *Polar Biol.* **16**, 271–286 (1996).
- 560 6. Barbraud, C. *et al.* Contrasted demographic responses facing future climate change in Southern Ocean
561 seabirds: Seabird demography and climate change. *J. Anim. Ecol.* **80**, 89–100 (2011).
- 562 7. Croxall, J. P., Trathan, P. N. & Murphy, E. J. Environmental Change and Antarctic Seabird Populations.
563 *Science* **297**, 1510–1514 (2002).
- 564 8. Costello, M. J. *et al.* Biodiversity Hotspots. in *Climate Change 2022 – Impacts, Adaptation and Vulnerability*
565 2123–2162 (Cambridge University Press, 2023). doi:10.1017/9781009325844.018.
- 566 9. Chown, S. L. *et al.* Antarctic climate change and the environment: A decadal synopsis and recommendations
567 for action. *Sci. Comm. Antarct. Res. Camb. U. K.* (2022).
- 568 10. Attard, M. R. G. *et al.* Review of Satellite Remote Sensing and Unoccupied Aircraft Systems for Counting
569 Wildlife on Land. *Remote Sens.* **16**, 627 (2024).
- 570 11. Oppel, S. *et al.* Estimating population size of a nocturnal burrow-nesting seabird using acoustic monitoring
571 and habitat mapping. *Nat. Conserv.* **7**, 1–13 (2014).
- 572 12. Buxton, R. T., Major, H. L., Jones, I. L. & Williams, J. C. Examining patterns in nocturnal seabird activity and
573 recovery across the Western Aleutian Islands, Alaska, using automated acoustic recording. *The Auk* **130**,
574 331–341 (2013).
- 575 13. Duda, M. P. *et al.* Reconstructing Long-Term Changes in Avian Populations Using Lake Sediments: Opening
576 a Window Onto the Past. *Front. Ecol. Evol.* **9**, 698175 (2021).
- 577 14. Mills, W. F., Morley, T. I., Votier, S. C. & Phillips, R. A. Long-term inter- and intraspecific dietary variation in
578 sibling seabird species. *Mar. Biol.* **168**, 31 (2021).
- 579 15. Berrow, S. D. & Croxall, J. P. The diet of white-chinned petrels *Procellaria aequinoctialis*, Linnaeus 1758, in
580 years of contrasting prey availability at South Georgia. *Antarct. Sci.* **11**, 283–292 (1999).
- 581 16. Ceia, F. R. *et al.* Short- and long-term consistency in the foraging niche of wandering albatrosses. *Mar. Biol.*
582 **159**, 1581–1591 (2012).
- 583 17. Groff, D. V. *et al.* Seabird establishment during regional cooling drove a terrestrial ecosystem shift 5000
584 years ago. *Sci. Adv.* **6**, eabb2788 (2020).
- 585 18. Martín-Vélez, V. *et al.* Quantifying nutrient inputs by gulls to a fluctuating lake, aided by movement ecology
586 methods. *Freshw. Biol.* **64**, 1821–1832 (2019).
- 587 19. Roberts, S. J. *et al.* Past penguin colony responses to explosive volcanism on the Antarctic Peninsula. *Nat.*
588 *Commun.* **8**, 14914 (2017).
- 589 20. Xu, L. *et al.* Decline of recent seabirds inferred from a composite 1000-year record of population dynamics.
590 *Sci. Rep.* **6**, 35191 (2016).
- 591 21. Liu, X. D. *et al.* Geochemical evidence for the variation of historical seabird population on Dongdao Island
592 of the South China Sea. *J. Paleolimnol.* **36**, 259–279 (2006).
- 593 22. Duda, M. P. *et al.* Striking centennial-scale changes in the population size of a threatened seabird. *Proc. R.*
594 *Soc. B Biol. Sci.* **287**, 20192234 (2020).
- 595 23. Duda, M. P. *et al.* Linking 19th century European settlement to the disruption of a seabird's natural
596 population dynamics. *Proc. Natl. Acad. Sci.* **117**, 32484–32492 (2020).
- 597 24. Duda, M. P. *et al.* A 2200-year record of Andean Condor diet and nest site usage reflects natural and
598 anthropogenic stressors. *Proc. R. Soc. B Biol. Sci.* **290**, 20230106 (2023).
- 599 25. Davidson, T. A. *et al.* The history of seabird colonies and the North Water ecosystem: Contributions from
600 palaeoecological and archaeological evidence. *Ambio* **47**, 175–192 (2018).
- 601 26. Liu, X. *et al.* A preliminary record of the historical seabird population in the Larsemann Hills, East Antarctica,
602 from geochemical analyses of Mochou Lake sediments. *Boreas* **36**, 182–197 (2007).
- 603 27. Zheng, W., Xie, Z. & Bergquist, B. A. Mercury Stable Isotopes in Ornithogenic Deposits As Tracers of
604 Historical Cycling of Mercury in Ross Sea, Antarctica. *Environ. Sci. Technol.* **49**, 7623–7632 (2015).

- 605 28. Outridge, P. M., Goodsite, M. E., Bennike, O., Rausch, N. & Shotyk, W. Seabird Transfer of Nutrients and
606 Trace Elements from the North Water Polynya to Land during the Mid-Holocene Warm Period, Carey
607 Islands, Northwest Greenland + Supplementary Appendix Figure S1 (See Article Tools). *ARCTIC* **69**, 253
608 (2016).
- 609 29. Anderson, O. *et al.* Influence of trophic position and foraging range on mercury levels within a seabird
610 community. *Mar. Ecol. Prog. Ser.* **375**, 277–288 (2009).
- 611 30. Mills, W. F., Bustamante, P., Ramírez, F., Forero, M. G. & Phillips, R. A. Mercury Concentrations in Feathers
612 of Albatrosses and Large Petrels at South Georgia: Contemporary Patterns and Comparisons with Past
613 Decades. *Arch. Environ. Contam. Toxicol.* **86**, 363–374 (2024).
- 614 31. Sun, L. G. *et al.* Vertebrate records in polar sediments: Biological responses to past climate change and
615 human activities. *Earth-Sci. Rev.* **126**, 147–155 (2013).
- 616 32. Soares, T. A. *et al.* Ornithogenic mercury input to soils of Admiralty Bay, King George Island, Antarctica.
617 *Polar Biol.* **47**, 891–901 (2024).
- 618 33. Geizer, H. D., Klapstein, S. J., Mallory, M. L. & O’Driscoll, N. J. Total mercury, methylmercury, phosphate,
619 and sulfate inputs to a bog ecosystem from herring gull (*Larus smithsonianus*) guano. *Ecotoxicol. Environ.*
620 *Saf.* **226**, 112845 (2021).
- 621 34. Li, C. *et al.* A peat core Hg stable isotope reconstruction of Holocene atmospheric Hg deposition at
622 Amsterdam Island (37.8oS). *Geochim. Cosmochim. Acta* **341**, 62–74 (2023).
- 623 35. Enrico, M. *et al.* Atmospheric Mercury Transfer to Peat Bogs Dominated by Gaseous Elemental Mercury Dry
624 Deposition. *Environ. Sci. Technol.* **50**, 2405–2412 (2016).
- 625 36. Liu, Y. *et al.* Understanding foliar accumulation of atmospheric Hg in terrestrial vegetation: Progress and
626 challenges. *Crit. Rev. Environ. Sci. Technol.* 1–22 (2021) doi:10.1080/10643389.2021.1989235.
- 627 37. Woerndle, G. E. *et al.* New Insights on Ecosystem Mercury Cycling Revealed by Stable Isotopes of Mercury
628 in Water Flowing from a Headwater Peatland Catchment. *Environ. Sci. Technol.* **52**, 1854–1861 (2018).
- 629 38. Liem-Nguyen, V., Skyllberg, U. & Björn, E. Thermodynamic Modeling of the Solubility and Chemical
630 Speciation of Mercury and Methylmercury Driven by Organic Thiols and Micromolar Sulfide Concentrations
631 in Boreal Wetland Soils. *Environ. Sci. Technol.* **51**, 3678–3686 (2017).
- 632 39. Jiang, T. *et al.* Modeling of the structure-specific kinetics of abiotic, dark reduction of Hg(II) complexed by
633 O/N and S functional groups in humic acids while accounting for time-dependent structural rearrangement.
634 *Geochim. Cosmochim. Acta* **154**, 151–167 (2015).
- 635 40. Li, C. *et al.* Perspectives on using peat records to reconstruct past atmospheric Hg levels. *J. Hazard. Mater.*
636 **482**, 136581 (2025).
- 637 41. Clarke, A., Croxall, J. P., Poncet, S., Martin, A. R. & Burton, R. Important bird areas: South Georgia. *Br. Birds*
638 118–144 (2012).
- 639 42. Smith, R. I. L. Terrestrial plant biology of the sub-Antarctic and Antarctic. in *Antarctic Ecology* 61–162
640 (Academic Press, London, 1984).
- 641 43. Lewis-Smith, R.I. Types of peat and peat-forming vegetation on South Georgia. *Br. Antarct. Surv. Bull.* **53**,
642 119–139.
- 643 44. Fenton, J. H. C. The contribution of Antarctic moss peat to the understanding of global peatland processes.
644 *Antarct. Sci.* **34**, 266–278 (2022).
- 645 45. Nielsen, S. H. H., Koç, N. & Crosta, X. Holocene climate in the Atlantic sector of the Southern Ocean:
646 Controlled by insolation or oceanic circulation? *Geology* **32**, 317 (2004).
- 647 46. Orme, L. C. *et al.* Sea surface temperature in the Indian sector of the Southern Ocean over the Late Glacial
648 and Holocene. *Clim. Past* **16**, 1451–1467 (2020).
- 649 47. Röthlisberger, R. *et al.* Dust and sea salt variability in central East Antarctica (Dome C) over the last 45 kyrs
650 and its implications for southern high-latitude climate. *Geophys. Res. Lett.* **29**, (2002).
- 651 48. Li, C. *et al.* Unequal Anthropogenic Enrichment of Mercury in Earth’s Northern and Southern Hemispheres.
652 *ACS Earth Space Chem.* **4**, 2073–2081 (2020).
- 653 49. Whittle, A. *et al.* Salt-Enrichment Impact on Biomass Production in a Natural Population of Peatland
654 Dwelling Arcellinida and Euglyphida (Testate Amoebae). *Microb. Ecol.* **78**, 534–538 (2019).
- 655 50. Whittle, A. Late Quaternary changes in the Westerly Winds over the Southern Ocean. (University of Exeter,
656 2021).
- 657 51. Kickbush, J. C. *et al.* The influence of avian biovectors on mercury speciation in a bog ecosystem. *Sci. Total*
658 *Environ.* **637–638**, 264–273 (2018).
- 659 52. Sprovieri, F. *et al.* Atmospheric mercury concentrations observed at ground-based monitoring sites globally
660 distributed in the framework of the GMOS network. *Atmospheric Chem. Phys.* **16**, 11915–11935 (2016).

- 661 53. Jitaru, P. *et al.* Atmospheric depletion of mercury over Antarctica during glacial periods. *Nat. Geosci.* **2**, 505–
662 508 (2009).
- 663 54. Blum, J. D., Sherman, L. S. & Johnson, M. W. Mercury Isotopes in Earth and Environmental Sciences. *Annu.*
664 *Rev. Earth Planet. Sci.* **42**, 249–269 (2014).
- 665 55. Bergquist, B. A. & Blum, J. D. Mass-Dependent and -Independent Fractionation of Hg Isotopes by
666 Photoreduction in Aquatic Systems. *Science* **318**, 417–420 (2007).
- 667 56. Enrico, M. *et al.* Holocene Atmospheric Mercury Levels Reconstructed from Peat Bog Mercury Stable
668 Isotopes. *Environ. Sci. Technol.* **51**, 5899–5906 (2017).
- 669 57. Li, C. *et al.* Mercury deposition and redox transformation processes in peatland constrained by mercury
670 stable isotopes. *Nat. Commun.* **14**, 7389 (2023).
- 671 58. Zheng, W. & Hintelmann, H. Isotope Fractionation of Mercury during Its Photochemical Reduction by Low-
672 Molecular-Weight Organic Compounds. *J. Phys. Chem. A* **114**, 4246–4253 (2010).
- 673 59. Zheng, W. & Hintelmann, H. Nuclear Field Shift Effect in Isotope Fractionation of Mercury during Abiotic
674 Reduction in the Absence of Light. *J. Phys. Chem. A* **114**, 4238–4245 (2010).
- 675 60. Médiéu, A. *et al.* Mercury Stable Isotopes Reveal the Vertical Distribution and Trophic Ecology of Deep-
676 Pelagic Organisms over the North-East Atlantic Ocean Continental Slope. *Environ. Sci. Technol.* **58**, 18733–
677 18743 (2024).
- 678 61. Motta, L. C. *et al.* Mercury Cycling in the North Pacific Subtropical Gyre as Revealed by Mercury Stable
679 Isotope Ratios. *Glob. Biogeochem. Cycles* **33**, 777–794 (2019).
- 680 62. Yuan, W. *et al.* Stable Isotope Evidence Shows Re-emission of Elemental Mercury Vapor Occurring after
681 Reductive Loss from Foliage. *Environ. Sci. Technol.* **53**, 651–660 (2019).
- 682 63. Smith, V. R. Production and nutrient dynamics of plant communities on a sub-Antarctic Island: 5. Nutrient
683 budget and turnover times for mire-grasslands, fjaldmark and fernbrakes. *Polar Biol.* **8**, 255–269 (1988).
- 684 64. von Scheffer, C., Mauquoy, D., Theurer, T., Coathup, D. & Muirhead, D. ‘Fire Islands’: Holocene wildfire
685 intensity as a critical determinant of carbon accumulation in South Atlantic peatlands. Preprint at
686 <https://doi.org/10.5281/ZENODO.17171935> (2025).
- 687 65. Gallego-Sala, A. V. *et al.* Latitudinal limits to the predicted increase of the peatland carbon sink with
688 warming. *Nat. Clim. Change* **8**, 907–913 (2018).
- 689 66. Payne, R. J. *et al.* Peatland initiation and carbon accumulation in the Falkland Islands. *Quat. Sci. Rev.* **212**,
690 213–218 (2019).
- 691 67. Smith, R. I. L. & Clymo, R. S. An extraordinary peat-forming community on the Falkland Islands. *Nature* **309**,
692 617–620 (1984).
- 693 68. Otero, X. L., De La Peña-Lastra, S., Pérez-Alberti, A., Ferreira, T. O. & Huerta-Díaz, M. A. Seabird colonies as
694 important global drivers in the nitrogen and phosphorus cycles. *Nat. Commun.* **9**, 246 (2018).
- 695 69. Chen, J., Hintelmann, H., Feng, X. & Dimock, B. Unusual fractionation of both odd and even mercury isotopes
696 in precipitation from Peterborough, ON, Canada. *Geochim. Cosmochim. Acta* **90**, 33–46 (2012).
- 697 70. Osman, M. B. *et al.* Globally resolved surface temperatures since the Last Glacial Maximum. *Nature* **599**,
698 239–244 (2021).
- 699 71. Thorne, L., Clay, T., Phillips, R., Silvers, L. & Wakefield, E. Effects of wind on the movement, behavior,
700 energetics, and life history of seabirds. *Mar. Ecol. Prog. Ser.* **723**, 73–117 (2023).
- 701 72. Cairns, D. K. Seabirds as Indicators of Marine Food Supplies. *Biol. Oceanogr.* **5**, 261–271 (1988).
- 702 73. Froy, H. *et al.* Age-Related Variation in Foraging Behaviour in the Wandering Albatross at South Georgia: No
703 Evidence for Senescence. *PLOS ONE* **10**, e0116415 (2015).
- 704 74. Granroth-Wilding, H. M. V. & Phillips, R. A. Segregation in space and time explains the coexistence of two
705 sympatric sub-Antarctic petrels. *Ibis* **161**, 101–116 (2019).
- 706 75. Phillips, R. A., Silk, J. R. D., Croxall, J. P. & Afanasyev, V. Year-round distribution of white-chinned petrels
707 from South Georgia: Relationships with oceanography and fisheries. *Biol. Conserv.* **129**, 336–347 (2006).
- 708 76. Wakefield, E. D. *et al.* Seasonal resource tracking and use of sea-ice foraging habitats by albatrosses and
709 large petrels. *Prog. Oceanogr.* **230**, 103334 (2025).
- 710 77. Thorpe, S. E., Murphy, E. J. & Watkins, J. L. Circumpolar connections between Antarctic krill (*Euphausia*
711 *superba* Dana) populations: Investigating the roles of ocean and sea ice transport. *Deep Sea Res. Part*
712 *Oceanogr. Res. Pap.* **54**, 792–810 (2007).
- 713 78. Flores, H. *et al.* Impact of climate change on Antarctic krill. *Mar. Ecol. Prog. Ser.* **458**, 1–19 (2012).
- 714 79. Bestley, S. *et al.* Marine Ecosystem Assessment for the Southern Ocean: Birds and Marine Mammals in a
715 Changing Climate. *Front. Ecol. Evol.* **8**, 566936 (2020).
- 716 80. Brierley, A. S. *et al.* Antarctic Krill Under Sea Ice: Elevated Abundance in a Narrow Band Just South of Ice
717 Edge. *Science* **295**, 1890–1892 (2002).

- 718 81. Collins, M. A. *et al.* Mitigating the impact of longline fisheries on seabirds: Lessons learned from the South
719 Georgia Patagonian toothfish fishery (CCAMLR Subarea 48.3). *Mar. Policy* **131**, 104618 (2021).
- 720 82. Phillips, R. A. & Waluda, C. M. Albatrosses and petrels at South Georgia as sentinels of marine debris input
721 from vessels in the southwest Atlantic Ocean. *Environ. Int.* **136**, 105443 (2020).
- 722 83. Martin, A. R. & Richardson, M. G. Rodent eradication scaled up: clearing rats and mice from South Georgia.
723 *Oryx* **53**, 27–35 (2019).
- 724 84. Swart, N. C. & Fyfe, J. C. Observed and simulated changes in the Southern Hemisphere surface westerly
725 wind-stress. *Geophys. Res. Lett.* **39**, 2012GL052810 (2012).
- 726 85. Holmes, C., Doddridge, E. & Fretwell, P. Antarctic Sea Ice #4: Record lows between 2022 and 2025. (2025)
727 doi:10.48361/KVK6-ZX15.
- 728 86. Richards, P. & Tickell, W. Comparison between the weather at bird island and King Edward Point, South
729 Georgia. *Br. Antarct. Surv. Bull.* (1968).
- 730 87. Bannister, D. & King, J. C. The characteristics and temporal variability of föhn winds at King Edward Point,
731 South Georgia. *Int. J. Climatol.* **40**, 2778–2794 (2020).
- 732 88. Scaife, R. G. *et al.* The Falkland Islands’ palaeoecological response to millennial-scale climate perturbations
733 during the Pleistocene–Holocene transition: Implications for future vegetation stability in the southern
734 ocean islands. *J. Quat. Sci.* **34**, 609–620 (2019).
- 735 89. De Vleeschouwer, F., Chambers, F. M. & Swindles, G. T. Coring and sub-sampling of peatlands for
736 palaeoenvironmental research. *Mires Peat* **1819–754X**, (2010).
- 737 90. Mauquoy, D. & Van Geel, B. PLANT MACROFOSSIL METHODS AND STUDIES | Mire and Peat Macros. in
738 *Encyclopedia of Quaternary Science* 637–656 (Elsevier, 2013). doi:10.1016/B978-0-444-53643-3.00206-5.
- 739 91. Blaauw, M. & Christen, J. A. Flexible paleoclimate age-depth models using an autoregressive gamma
740 process. *Bayesian Anal.* **6**, (2011).
- 741 92. Charman, D. J. *et al.* Climate-related changes in peatland carbon accumulation during the last millennium.
742 *Biogeosciences* **10**, 929–944 (2013).
- 743 93. Heiri, O., Lotter, A. F. & Lemcke, G. Loss on ignition as a method for estimating organic and carbonate
744 content in sediments: reproducibility and comparability of results. *J. Paleolimnol.* **25**, 101–110 (2001).
- 745 94. Enrico, M., Balcom, P., Johnston, D. T., Foriel, J. & Sunderland, E. M. Simultaneous combustion preparation
746 for mercury isotope analysis and detection of total mercury using a direct mercury analyzer. *Anal. Chim.*
747 *Acta* **1154**, 338327 (2021).
- 748 95. Blum, J. D. & Bergquist, B. A. Reporting of variations in the natural isotopic composition of mercury. *Anal.*
749 *Bioanal. Chem.* **388**, 353–359 (2007).
- 750 96. Demers, J. D., Blum, J. D. & Zak, D. R. Mercury isotopes in a forested ecosystem: Implications for air-surface
751 exchange dynamics and the global mercury cycle: MERCURY ISOTOPES IN A FORESTED ECOSYSTEM. *Glob.*
752 *Biogeochem. Cycles* **27**, 222–238 (2013).
- 753 97. Scanlon, T. M. *et al.* Mercury Accumulation in Tree Rings: Observed Trends in Quantity and Isotopic
754 Composition in Shenandoah National Park, Virginia. *J. Geophys. Res. Biogeosciences* **125**, (2020).
- 755

Supplementary Files

This is a list of supplementary files associated with this preprint. Click to download.

- [Lietal.toNat.Communsupplementaryinformation.pdf](#)